



City Research Online

City, University of London Institutional Repository

Citation: Karim, M. R., Ahmad, H., Ghosh, S. & Rahman, B. M. (2018). Mid-infrared supercontinuum generation using As₂Se₃ photonic crystal fiber and the impact of higher-order dispersion parameters on its supercontinuum bandwidth. *Optical Fiber Technology*, 45, pp. 255-266. doi: 10.1016/j.yofte.2018.07.024

This is the accepted version of the paper.

This version of the publication may differ from the final published version.

Permanent repository link: <https://openaccess.city.ac.uk/id/eprint/20499/>

Link to published version: <https://doi.org/10.1016/j.yofte.2018.07.024>

Copyright: City Research Online aims to make research outputs of City, University of London available to a wider audience. Copyright and Moral Rights remain with the author(s) and/or copyright holders. URLs from City Research Online may be freely distributed and linked to.

Reuse: Copies of full items can be used for personal research or study, educational, or not-for-profit purposes without prior permission or charge. Provided that the authors, title and full bibliographic details are credited, a hyperlink and/or URL is given for the original metadata page and the content is not changed in any way.

City Research Online:

<http://openaccess.city.ac.uk/>

publications@city.ac.uk

Mid-infrared supercontinuum generation using As₂Se₃ photonic crystal fiber and the impact of higher-order dispersion parameters on its supercontinuum bandwidth

M. R. Karim^a, H. Ahmad^{a,b}, Souvik Ghosh^c, B. M. A. Rahman^c

^aPhotonics Research Centre, University of Malaya, 50603 Kuala Lumpur, Malaysia

^bVisiting Professor at the Department of Physics, Faculty of Science and Technology, Airlangga University, Surabaya 60115, Indonesia

^cDepartment of Electrical and Electronic Engineering, City University of London, Northampton Square, London, EC1V 0HB, UK

Abstract

A dispersion engineered As₂Se₃ chalcogenide hexagonal photonic crystal fiber which can produce mid-infrared supercontinuum (SC) spectral evolution spanning from 2 μm to beyond 15 μm with a low peak power of 3 kW is numerically designed and demonstrated. Numerical analysis is carried out to investigate the impact of higher-order dispersion (HOD) parameters on the output SC bandwidth. Numerical analysis shows that the SC spectral broadening at the output of the proposed design depends on the convergence of the Taylor approximation with increasing fitting parameters, which implies a sufficient number of HOD parameters must be included during numerical simulations. Four designs with different structural parameters are optimized for pumping each operating at a different pump wavelength to test the convergence of output SC by the successive addition of HOD parameters. To realize spurious free SC spectral evolution by the proposed designs, HOD terms up to the sixteenth-order are included during all SC simulations. The proposed design can be used in molecular finger print spectroscopy, bio-medical imaging as well as various mid-infrared region applications.

Keywords: Numerical approximation and analysis, Nonlinear optics, Dispersion, Chalcogenide, Photonic crystal fiber, Supercontinuum generation

1. Introduction

Mid-infrared (MIR) spectral region (2-20 μm) supercontinuum (SC) generation has recently become the focus of considerable interest owing to its diverse applications in optical coherence tomography, biomedical imaging, high precision frequency metrology and molecular finger print spectroscopy [1, 2]. Almost all molecules in this region undergo strong vibrational absorption, providing significant pathways for MIR spectroscopy to trace and quantify the molecular species in a certain atmospheric condition [3]. Two vital spectral windows, at 3–5 μm and 8–13 μm are located in this region in which the atmosphere is relatively transparent and can thus be used to detect the scent of exotic/toxic gases that are detrimental for a multitude of industrial and atmospheric applications [4].

In order to produce ultrabroadband SC sources with high brightness that can cover the spectral evolution up to the molecular fingerprint region, researchers have proposed the use of optical waveguides made with different host materials such as fluoride, tellurite and chalcogenide glasses [5, 6, 7, 8, 9, 10, 11, 12, 13]. The MIR transparencies of fluoride and tellurite glasses are not more than 5 μm [14] and until to date the highest SC extension in the long wavelength edge by these two materials are 6.28 μm [15] and 4.87 μm [16], respectively. At the same time, chalcogenide (ChG) glasses have shown wider MIR transparency

exceeding 20 μm , depending on the compositions of glass components. These glasses possess high third-order Kerr nonlinearity which is hundreds of times larger than that of fluoride and tellurite glass, making more suitable as host materials for waveguide fabrication than most other materials with significant promise for MIR region applications [17, 18, 19, 20, 21, 22, 23, 24, 25, 26, 27, 28, 29, 30].

A number of numerical and experimental ultrabroadband SC spectra in the MIR region using ChG waveguides and fibers have been demonstrated quite recently [4, 10, 11, 12, 13, 14, 31, 32, 33]. Yu *et al.* [12] demonstrated a SC spectrum covering a wavelength range from 1.8 to 10 μm with a pulse duration of 330-fs pumped at 4 μm in a 11-cm long ChG step-index fiber using Ge₁₂As₂₄Se₆₄ as a core and Ge₁₂As₂₄S₆₄ for its outer cladding with an input peak power of 3 kW. The same research group also experimentally demonstrated in the following year SC generation covering a spectral range of 2-10 μm by an all-ChG rib waveguide made using GeAsSe glass as the core and Ge-AsS glass as both the upper and lower claddings with 330-fs pulses pumped at 4.184 μm with an input peak power of 4.5 kW [10]. Petersen *et al.* [11] reported a MIR SC spectra spanning from 1.4 μm to 13.3 μm with a 85-mm-long ChG step-index fiber made using As₄₀Se₆₀ as the core and Ge₁₀As_{23.5}Se_{66.6} glass for its outer cladding, pumped at 6.3 μm with pulses of 100-fs duration and an input peak power of 2.29 MW. Ou *et al.* [14] reported a MIR SC spec-

tral evolution up to 14 μm with a 20-cm-long ChG step-index fiber made using $\text{Ge}_{15}\text{Sb}_{25}\text{Se}_{60}$ glass as the core and $\text{Ge}_{12}\text{Sb}_{20}\text{Se}_{65}$ glass for its cladding, pumped with a 150-fs pulse duration at 6 μm and a peak power of 750 kW. Similarly, Cheng *et al.* [13] reported a MIR SC spectrum spanning the wavelength range 2–15.1 μm in a 3-cm-long ChG step-index fiber using As_2Se_3 as the core and AsSe_2 as outer cladding when pumped with a 170-fs pulses in 9.8 μm with a peak power of 2.89 MW, while Zhao *et al.* [4] demonstrated a MIR SC spectra extending up to 16 μm using a 14-cm-long step-index fiber made from Ge-Te-AgI glass when pumped at 7 μm with 150-fs duration pulses and a pulse repetition rate of 1 kHz with a peak power of 77 MW. Petersen *et al.* [31] experimentally demonstrates a broadband MIR SC generation spectra covering the wavelength from 1 to 11.5 μm with a high average output power above 4.5 μm in tapered large-mode-area ChG $\text{Ge}_{11}\text{As}_{22}\text{Se}_{68}$ photonic crystal fiber (PCF). Hudson *et al.* [32] reported a broadband MIR SC spectrum spanning from 1.8 to 9.5 μm using a $\text{As}_2\text{Se}_3/\text{As}_2\text{S}_3$ tapered fiber by launching 230-fs pulses with a pulse peak power of 4.2 kW, and Saini *et al.* [33] numerically demonstrated MIR SC generation covering a wavelength range 2–15 μm in a 5-mm long triangular core graded index As_2Se_3 PCF when pumped at 4.1 μm with a largest peak power of 3.5 kW. Wang *et al.* [34] recently reported MIR region SC generation covering a wavelength from 2 to 12.7 μm using a 12-cm long step-index fiber using As_2Se_3 as the core and $\text{As}_2\text{Se}_2\text{S}$ as the outer cladding using a pump at 6.5 μm with a pulse of 150-fs duration and a peak power of 93 MW. As alternative to index guiding microstructured fibers, recently developed hybrid/hollow-core bandgap guiding PCFs have also attracted considerable attention among the researchers owing to their inherent ability to integrate with different fluids, solids, and gases. This can significantly extend the functionality of these fibers and a broadband SC can be produced between the ultraviolet and the MIR region by optimizing dispersion and nonlinearity of the PCFs [35]. Habib *et al.* [36] numerically reported soliton-plasma interaction in a noble-gas-filled silica hollow-core anti-resonant hybrid PCF that was capable of producing a SC spectra in the range 1–4 μm when pumped at 3 μm .

Based on the afore-mentioned research works, it is apparent that researchers have been striving since the last decade to exploit ChG materials for generating long wavelength SC spectral evolutions in the MIR region applications. To generate long wavelength edge SC spectra spanning up to the MIR region, fiber based geometries are still preferred over other structures owing to their design flexibilities that to be achieved while at the same time allowing for better management of dispersion. Among the fiber based structures, the PCF is the most prominent design as this structure can be tuned by simply changing the composition of the core/cladding glasses [38, 39, 40, 41, 42]. Furthermore, ChG based PCFs with a periodic air-hole arrangements can be easily fabricated using the Stack-

and-Draw method, which is particularly suitable for PCFs with a regular pitch. Alternatively, the extrusion principle can also be considered, which is suitable for PCFs made from soft glass material. This is because soft glasses, those based on ChGs can accept high dopant concentrations and also their optical and mechanical characteristics can modify more widely than silica glass. This also assists in fabrication of PCFs with a more intricate microstructure incorporating a high refractive index contrast and high nonlinear coefficient. [43].

Since As_2Se_3 glass is among several ChG glass compositions that have shown excellent optical transparency in the range 0.85–17.5 μm with an attenuation coefficient of less than 1 cm^{-1} [44], a conventional 20-mm-long hexagonal PCF is numerically proposed using As_2Se_3 glass for an ultrabroadband SC generation spanning far into the MIR region. Four PCF geometries are proposed by varying their structural parameters including the pitch (Λ) and relative hole size (d/Λ) for pumping at different wavelengths. The proposed designs are investigated for MIR region SC spectral evolution through the successive addition of higher-order dispersion (HOD) terms up to sixteenth-order. Among the four geometries optimized for pumping at different wavelengths, pumping between 3.1 μm and 4 μm would allow MIR SC spectral expansion spanning from 2 μm to beyond 15 μm to be observed by the proposed PCF designs. In previous planar waveguide designs, eighth-order HOD terms (β_8) are required to obtain stable and spurious free SC evolution at the waveguide output [45]. In the case of the proposed PCF designs of this work, the total number of HOD terms are observed to vary depending on the PCF structure to obtain a stable and steady SC spectral evolutions at the waveguide output, in this case up to 16th order HOD term (β_{16}) included for all numerical SC simulations.

2. Theoretical Model

A traditional hexagonal PCF made with an As_2Se_3 glass core and cladding comprising of hexagonal lattice of air-holes running along the length of the fiber is proposed for this work. In order to calculate the wavelength dependent linear refractive index of the As_2Se_3 glass over a wide frequency range, the following Sellmeier equation is used for numerical simulations [46]

$$n^2(\lambda) - 1 = \lambda^2 \left(\frac{2.234921^2}{\lambda^2 - 0.24164^2} + \frac{0.347441^2}{\lambda^2 - 19^2} + \frac{1.308575^2}{\lambda^2 - 4 \times 0.24164^2} \right), \quad (1)$$

where λ is calculated in micrometers.

The As_2Se_3 PCF is designed and optimized by varying its parameters through in-house computer code developed using a finite-element method (FEM) mode-solver [47, 49].

To obtain high accuracy modal solutions from the FEM solver, the PCF structure is represented by 720,000 first-order non-overlapping triangular elements in transverse directions. Perfectly matched layer (PML) conditions is assumed at the boundary surrounding the PCF structure to calculate confinement losses. For certain Λ and d/Λ values, the FEM mode-solver provides the mode propagation constant, $\beta(\omega)$ of the fundamental mode, H_x^{11} for the proposed design as a function of the optical angular frequency, which is subsequently used to evaluate the group-velocity dispersion (GVD) as a function of wavelength.

To study the generation of a SC evolution from short optical pulses launched into the optimized As_2Se_3 PCF, the generalized nonlinear Schrödinger equation (GNLSE) for single polarization is solved. This is a widely employed method for obtaining a pulse evolution inside the optical waveguide [1, 48]:

$$\frac{\partial}{\partial z} A(z, T) + \frac{\alpha}{2} A - \sum_{k \geq 2} \frac{i^{k+1}}{k!} \beta_k \frac{\partial^k A}{\partial T^k} = i\gamma \left(1 + \frac{i}{\omega_0} \frac{\partial}{\partial T} \right) \times \left(A(z, T) \int_{-\infty}^{\infty} R(T') |A(z, T - T')|^2 dT' \right), \quad (2)$$

The left hand and right hand sides of Eq. (2) respectively express the linear and nonlinear effects acting inside the PCF structure during the propagation of pulses. The electric field envelop, $A(z, T)$ moves at the group velocity $1/\beta_1$ ($T = t - \beta_1 z$) where β_k ($k \geq 2$) expresses the k th-order HOD parameter and ω_0 is the center angular frequency of pump source. The nonlinear coefficient is defined as $\gamma = n_2 \omega_0 / (c A_{\text{eff}})$ where c , A_{eff} and n_2 represent the speed of light in vacuum, mode-effective area and nonlinear refractive index, respectively. The parameter α represents the linear material absorption losses when light travels through it.

During the SC evolution inside the optical waveguide, intrapulse Raman scattering plays a vital role which includes both the delayed Raman contribution (h_R) and instantaneous electronic contribution (f_R) through the response function [48]

$$R(t) = (1 - f_R)\delta(t) + f_R h_R(t), \quad (3)$$

with the Raman contribution having the form

$$h_R(t) = \frac{\tau_1^2 + \tau_2^2}{\tau_1 \tau_2^2} \exp\left(-\frac{t}{\tau_2}\right) \sin\left(\frac{t}{\tau_1}\right). \quad (4)$$

In this case, the f_R value for As_2Se_3 glass is taken to be 0.148 and τ_1 and τ_2 considered to be 23-fs and 164.5-fs, respectively [50].

3. Results and Discussion

The proposed hexagonal PCF with an As_2Se_3 core surrounded by air-hole rings as an outer cladding along the length of a 20-mm-long fiber is optimized by varying its d

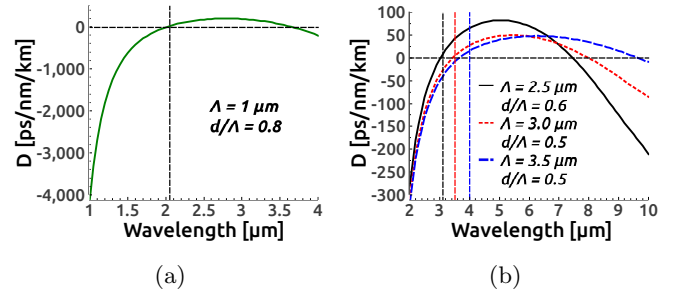


Figure 1: GVD curves of four As_2Se_3 PCF designs tailored for fundamental mode (H_x^{11}) by varying Λ and d/Λ for pumping at four different locations such as (a) 2.05 μm ; (b) 3.1 μm , 3.5 μm and 4 μm , respectively. Vertical dashed lines indicate pump wavelengths.

and Λ . As a result of higher leakage losses in the PCF with a fewer number of air-hole rings, five air-hole rings are incorporated for PCF modeling [51]. It should be noted that the additional air-hole rings do not significantly change the dispersion properties of the PCF, but only affects the leakage and bending losses. The PCF can be designed with strong confinement which results in high nonlinear interaction inside the core due to the high index contrast between the core and air-holes. A ChG based PCF with a high refractive index shows higher mode confinement which eventually induces a strong nonlinear interaction inside the waveguide due to its high Kerr nonlinearity. Apart from the Kerr effect, the GVD parameter also plays a vital role in producing an SC spectra by interacting with a multitude of nonlinear effects such as self-phase modulation (SPM), cross-phase modulation (XPM), Soliton, Raman effect and dispersive wave (DW) generation during

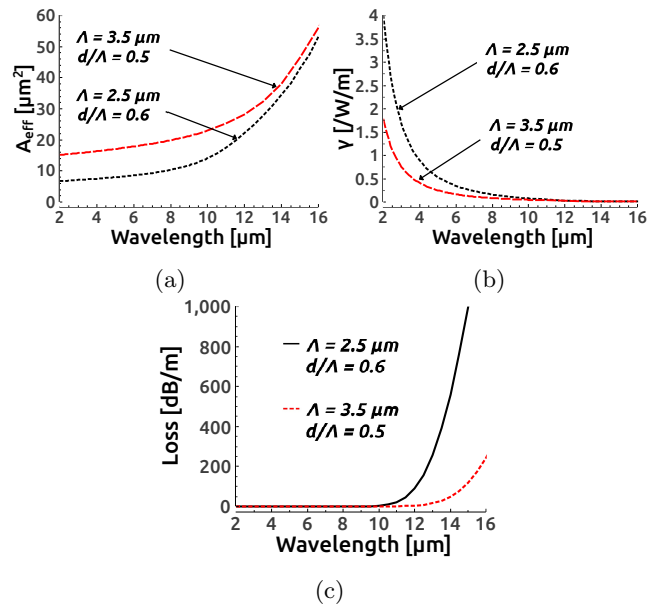


Figure 2: (a) Mode effective areas; (b) Nonlinear coefficients and (c) Confinement losses of fundamental mode are evaluated over a wide wavelength range for the PCF structures of $\Lambda = 2.5 \mu\text{m}$, $d/\Lambda = 0.6$ and $\Lambda = 3.5 \mu\text{m}$, $d/\Lambda = 0.5$, respectively.

ultra-short pulse propagation inside the waveguide structure. To obtain the SC spectral evolution extending up to the MIR, the GVD of the proposed design is tailored over a wide wavelength range so that a large frequency shift can be induced by forming Raman solitons inside the PCF structure.

Figure 1(a) shows a GVD curve tailored for a PCF geometry which is designed for pumping at $2.05 \mu\text{m}$ by setting its structural parameters so that $\Lambda = 1 \mu\text{m}$ and $d/\Lambda = 0.8$ from which the core diameter, $2\Lambda - d$ of the PCF can be calculated as $1.2 \mu\text{m}$. Figure 1(b) shows a set of GVD curves tailored to the wide anomalous dispersion regions by micro-structuring their Λ parameter to fall between $2.5 \mu\text{m}$ and $3.5 \mu\text{m}$ and d/Λ to fall between 0.5 and 0.6 for pumping at $3.1 \mu\text{m}$, $3.5 \mu\text{m}$ and $4 \mu\text{m}$, respectively. The core diameter of the last three designs are $3.5 \mu\text{m}$, $4.5 \mu\text{m}$ and $5.25 \mu\text{m}$, respectively. Four designs are optimized such that their 1st zero dispersion wavelengths (ZDWs) are located in the vicinity to the pump sources of each design. Among four PCF designs proposed, it would be challenging task to fabricate the 1st structure owing to its small core diameter as compared to the other three designs. To shift the ZDW of 1st PCF structure at $2 \mu\text{m}$ wavelength so as to overcome the large material dispersion of AsSe glass, which has a ZDW around at $7 \mu\text{m}$, the ratio d/Λ needs to be increased at 0.8 which enhances the fabrication difficulty of that design. Xing *et al.* [52, 53] reported a small core PCF design made of GeAsSe ChG glass for parametric conversions by shifting the PCF dispersion near the $2 \mu\text{m}$ region through micro-structuring and tapering the fiber while maintaining d/Λ ratio at ~ 0.7 . It was possible to obtain the ZDW with a lower d/Λ ratio for GeAsSe material owing to its lower material dispersion as compared to AsSe glass. Furthermore, tapering in this work offers added advantage of shifting the ZDW in the short wavelength region. Toupin *et al.* [54] proposed another small core PCF structure which was made from AsSe/GeAsSe ChG glasses by employing two-step drawing operation with additional optical losses as compared to single-step drawing processes. However, in this case, glasses with high stability against crystallization are required. Therefore, our proposed small core PCF structure with a core diameter of $1.2 \mu\text{m}$ can be fabricated through tapering and using two step drawing process which eventually may lower the d/Λ ratio, which is an important factor for dispersion tailoring of a design in the short wavelength region. The proposed PCF also shows a slight birefringence and the GVD curves shown in Fig. 1 are calculated for the H_x^{11} mode. The GVD parameters for the H_y^{11} mode are also calculated and compared with that of the H_x^{11} mode. No significant differences are observed between the GVD parameters obtained for the two different polarizations. However, the presence of small birefringence may result in a slight broadening variation of the SC at the PCF's output.

In order to realize a MIR SC evolution in the proposed PCF design, numerical simulations are carried out by solv-

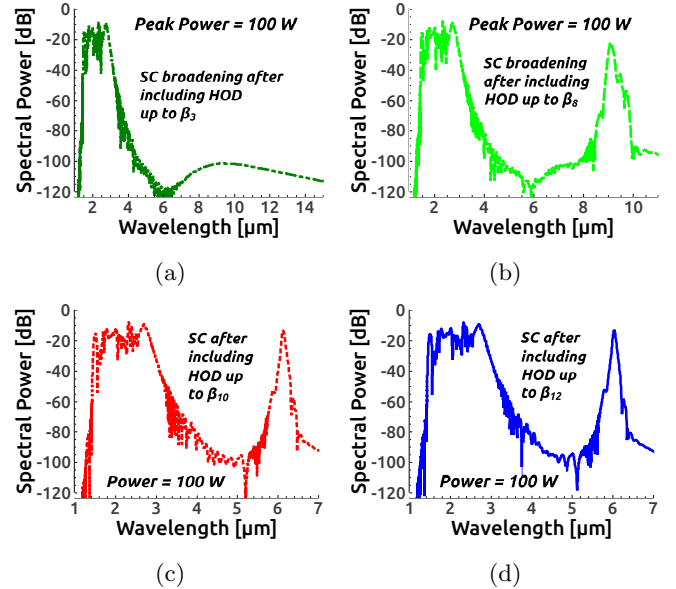


Figure 3: SC spectra at the output of As_2Se_3 PCF for the geometry of $\Lambda = 1.0 \mu\text{m}$ and $d/\Lambda = 0.8$ pumped at $2.05 \mu\text{m}$ for the HOD parameters from β_3 to β_{12} applying 100 W peak power at the PCF input.

ing the GNLSE Eq. (2) in a split-step Fourier method using the MATLAB software. Numerical simulations are carried out by taking 2^{17} grid points with minimum temporal resolution of 3.42-fs at a pump wavelength of $2.05 \mu\text{m}$ and between 5.17 and 6.67-fs at a pump wavelength between 3.1 and $4 \mu\text{m}$ so that the time window can accommodate extreme spectral broadening by avoiding negative frequency generation. The number of steps are taken as 100,000 with a step size of $0.2 \mu\text{m}$. A sech pulse with a 100-fs duration and peak pulse power between 100 W and 3 kW is launched into the proposed design at a wavelength between $2.05 \mu\text{m}$ and $4 \mu\text{m}$. This is realized through the use of tunable Raman soliton fluoride fiber lasers with a range $2\text{--}4.3 \mu\text{m}$ [55]. The mode-effective areas of the proposed PCF structures are calculated using the FEM mode-solver and their corresponding nonlinear coefficients are evaluated by considering the nonlinear refractive index, $n_2 = 1.1 \times 10^{-17}$

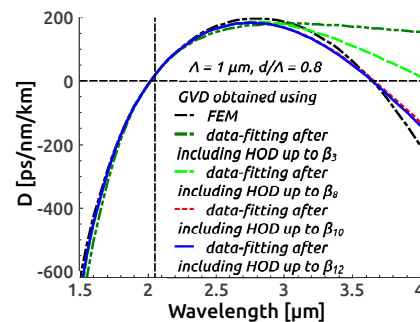


Figure 4: Comparison between actual GVD curve obtained by FEM mode-solver and data-fitted GVD curves obtained by Taylor-series expansion for the successive inclusion of HOD terms from β_3 to β_{12} . Vertical dashed line indicates pump wavelength.

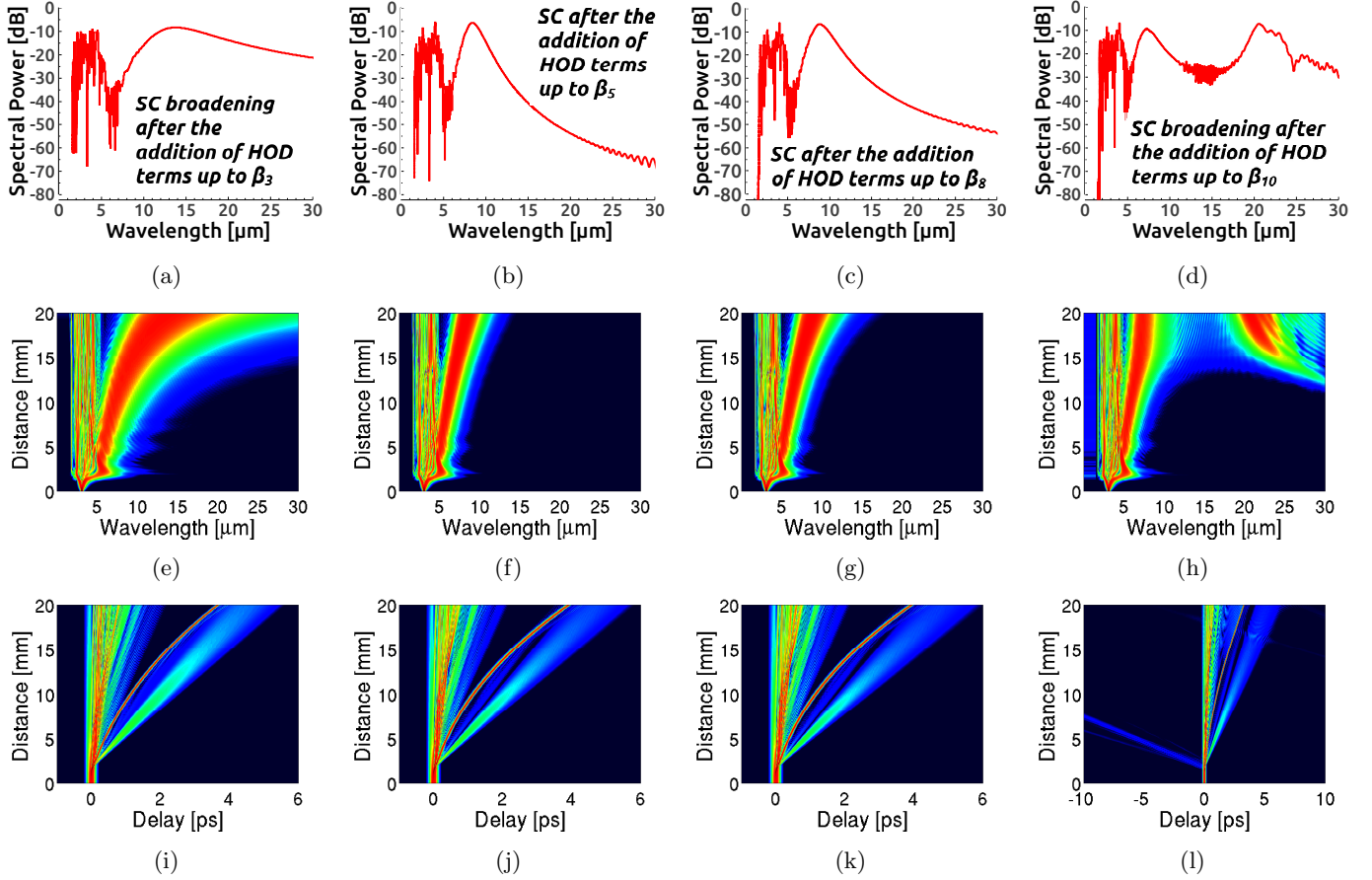


Figure 5: SC spectra (top row) and their corresponding spectral and temporal evolutions (middle and bottom rows, respectively) for 20-mm-long As_2Se_3 PCF geometry of $\Lambda = 2.5 \mu\text{m}$, $d/\Lambda = 0.6$ when pumped at $3.1 \mu\text{m}$ with a peak power of 3 kW for the HOD parameters of β_3 (extreme left column), β_5 (2nd column), β_8 (3rd column) and β_{10} (extreme right column), respectively.

m^2/W [13, 38] although Shiryayev *et al.* [44] reported $n_2 = (1.4 - 3) \times 10^{-17} \text{m}^2/\text{W}$ which is more than the value considered in the numerical simulations. Mode effective areas and their corresponding nonlinear coefficients are calculated and shown in Fig. 2(a) and 2(b) for Λ between 2.5 and $3.5 \mu\text{m}$ and d/Λ between 0.5 and 0.6, respectively. Confinement losses of the above mentioned geometries are also shown in Fig. 2(c). Since the material absorption edge of As_2Se_3 glass in long wavelength region could not be obtained, a constant linear propagation loss of 0.65 dB/cm is considered, as is reported by Shiryayev *et al.* [44] for a mono-index As_2Se_3 glass fiber at a wavelength of $10.6 \mu\text{m}$. The calculated GVD values for the four designs at the pump wavelengths are 19.92 ps/nm/km, 8.19 ps/nm/km, 4.06 ps/nm/km and 15 ps/nm/km, respectively. The nonlinear coefficient for first PCF geometry, $\Lambda = 1.0 \mu\text{m}$ and $d/\Lambda = 0.8$ is calculated as 24.05 /W/m from the mode effective area of $1.06 \mu\text{m}^2$ which is obtained at the pump wavelength. From the dispersion length, L_D and nonlinear length, L_{NL} , the soliton order, N can be calculated as ~ 13 for the first optimized PCF design. The SC dynamics inside the PCF after launching an ultrashort pump pulse into the waveguide with consecutive inclusion of different number of HOD terms during numerical simulations are

explained in later sections.

To observe SC spectral broadening and to gauge the impact of the HOD parameters on the SC bandwidth at the optimized design output, a sech pulse with a duration of 100-fs and a peak power of 100 W is initially launched into the first PCF design at a pump wavelength of $2.05 \mu\text{m}$. Numerical simulations are carried out using the optimized design by including HOD terms up to β_3 , giving the SC spectrum shown in Fig. 3(a). With the inclusion of the HOD terms up to β_3 , SC broadening up to 3100 nm is observed, spanning a range from 1400 to 3100 nm at -20 dB level from the peak. Further inclusion of HOD terms up to β_8 show a narrowband long wavelength DW is generated with a center peak at the $9 \mu\text{m}$ region as seen in Fig. 3(b). Subsequent addition of HOD terms up to β_{10} and β_{12} , as shown in Fig. 3(c) and 3(d) demonstrate that the DW induced into the SC spectra becomes steady and converges at $6.5 \mu\text{m}$ after the inclusion of HOD terms up to the β_{10} . Adding more HOD terms of up to β_{12} does not change the SC bandwidth further at the PCF output. Using a low peak power of 100 W, it is possible to obtain the SC expansion up to $6.5 \mu\text{m}$ as a result of PCF small core size, as this would help to induce large nonlinear coefficient inside the fiber. It must be observed also that

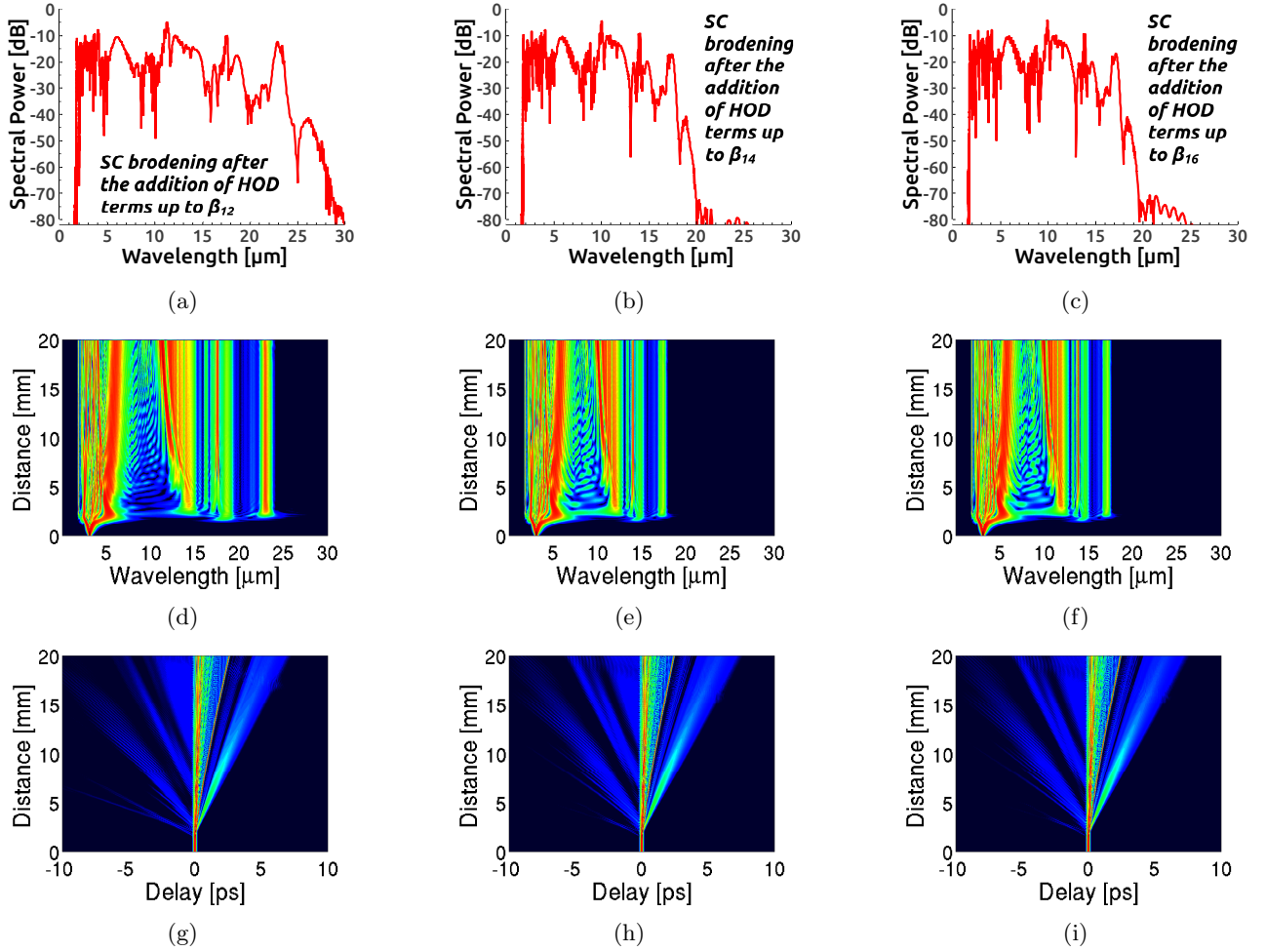


Figure 6: SC spectra (top row) and their corresponding spectral and temporal evolutions (middle and bottom rows, respectively) for 20-mm-long As_2Se_3 PCF geometry of $\Lambda = 2.5 \mu\text{m}$, $d/\Lambda = 0.6$ when pumped at $3.1 \mu\text{m}$ with a peak power of 3 kW for the HOD parameters of β_{12} (left column), β_{14} (middle column) and β_{16} (right column), respectively.

during the coupling process, difficulties may arise due to a small mode effective area (A_{eff}) of the fiber. As the A_{eff} of this design is smaller than the A_{eff} of a typical single mode fiber, higher coupling losses may be encountered, though this can be controlled by using a tapered spot-size converter during coupling between the pump source and the fiber. To verify the convergence of SC results at the PCF output, a comparison between the actual GVD curve obtained by the FEM solver and data-fitted GVD curves obtained through the successive addition of HOD terms from β_3 to β_{10} is given in Fig. 4. It can be clearly seen from the figure that the data-fitted GVD curve more accurately represents the actual GVD curve after the inclusion of HOD terms up to β_{10} , while further inclusion of HOD terms up to β_{12} do not make any difference to the data-fitted GVD curve. Thus, the SC output bandwidth for this design can be converged with the inclusion of HOD terms up to β_{10} .

Subsequently, a PCF geometry containing the dimensional parameters, $\Lambda = 2.5 \mu\text{m}$ and $d/\Lambda = 0.6$ for pumping it at $3.1 \mu\text{m}$ with a pump peak power of 3 kW is optimized.

A MIR SC spectrum spanning from $2 \mu\text{m}$ to beyond $15 \mu\text{m}$ is generated with the addition of HOD terms up to β_{14} by this design. The nonlinear coefficient for this geometry is calculated as 1.61 /W/m from the mode effective area of $6.59 \mu\text{m}^2$ which is obtained at the pump wavelength. From the dispersion length, L_D and nonlinear length, L_{NL} , the soliton order, N can be calculated as ~ 17 for the optimized design. After including HOD terms of up to β_{10} in the simulation, the expansion of the SC evolution in the proposed PCF output can be observed from $2 \mu\text{m}$ to $25 \mu\text{m}$ at -20 dB from the peak, given in Fig. 5(d). In order to validate this result, a number of numerical simulations are carried out by the successive inclusion of HOD terms starting from β_3 as shown in Fig. 5. It is apparent from the top row of the figure that the output bandwidth of the SC spectrum changes up to the inclusion of β_{10} and their corresponding spectral and temporal evolutions along the length of the optimized 20-mm fiber structure can be observed in the middle and bottom rows, respectively. From the spectral and temporal density evolutions, it can be observed that soliton fission occurs at a distance of 2 mm along the length

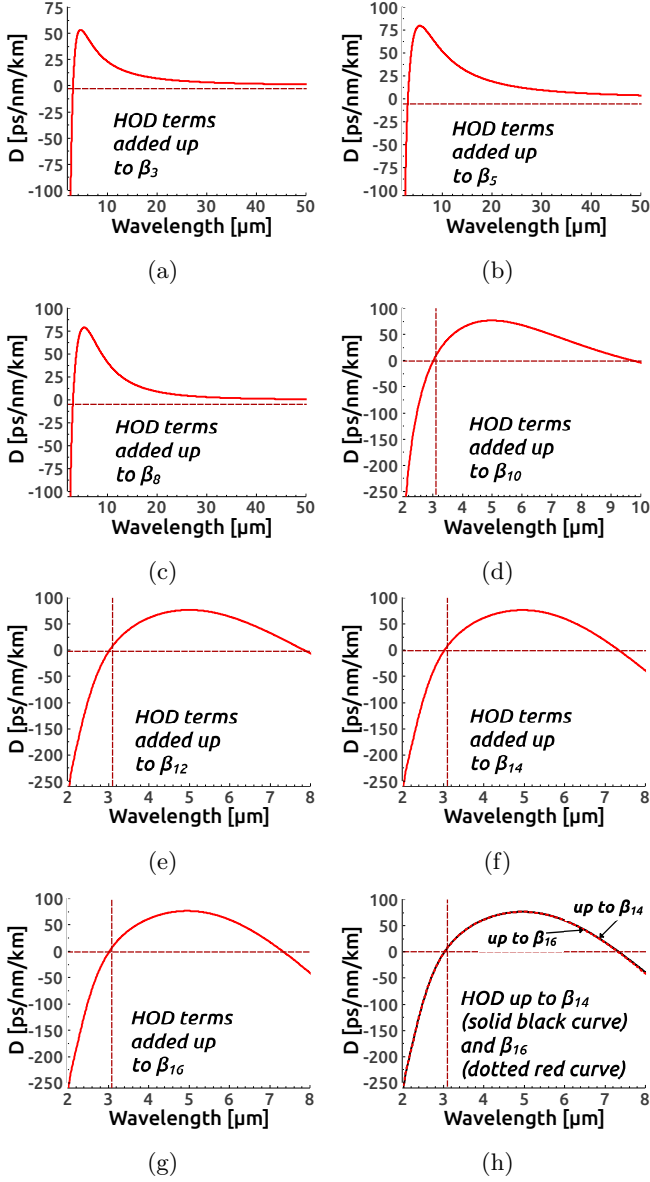


Figure 7: Data fitted GVD curves obtained by Taylor-series expansion which is corresponding to the GVD curve evaluated for the PCF geometry of $\Lambda = 2.5 \mu\text{m}$ and $d/\Lambda = 0.6$ (solid-black line in Fig. 1). Vertical dashed line indicates pump wavelength.

of the fiber. Before soliton fission, the SC is broadened symmetrically around the pump source by SPM. Through subsequent addition of HOD terms from β_3 to β_8 , it can be observed from spectral densities of Figs. 5(e-g) and temporal densities of 5(i-k) that 17 fundamental solitons are produced by soliton fission process which induced multiple spectral peaks on the spectra. One strong red shifted soliton along with other low energy solitons is observed to have moved towards the Stokes side or long wavelength region owing to Raman induced frequency shifts which produced a large spectral peak in the long wavelength side of the spectra. In the anti-Stokes side or short wavelength region at around $2 \mu\text{m}$, a phase-matched narrow-band resonant DW is observed in the normal GVD regime, which

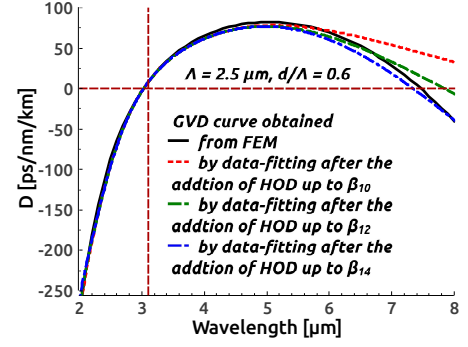


Figure 8: Comparison between data-fitted GVD curves and the actual GVD curve obtained by Taylor-series expansion and FEM mode-solver, respectively. Vertical dashed line indicates pump wavelength.

is induced by energy shedding from solitons owing to the presence of HOD terms. After the inclusion of HOD up to β_{10} , significant changes are observed in the SC spectral evolution in the long wavelength side. In this case, a large red shifted DW is induced owing to the inclusion of more HOD terms, which was expanded up to $25 \mu\text{m}$ as can be seen in Fig. 5(d). The corresponding spectral and temporal density evolutions that support this result can also be observed from Figs. 5(h) and 5(l), respectively.

In order to yield a steady SC output from our proposed design, the HOD terms up to β_{16} from the GVD curves are evaluated and given in Fig. 1(b). Figure 6 illustrates the SC spectra obtained by the inclusion of HOD terms β_{12} to β_{16} . It is observed that a significant variation in the SC output spectrum shape between β_{10} and β_{12} can be seen in Figs. 5 (extreme right column) and 6 (left column). A spectrum spanning up to $25 \mu\text{m}$ observed after the addition of β_{12} can be seen in Fig. 6(a). Including the HOD terms of up to β_{14} and β_{16} , two separate simulations are performed and their results are shown by middle and right columns in Fig. 6. It can be noticed from the middle column of Fig. 6 that the SC spectrum gets narrower than earlier inclusion (up to β_{12} as shown in left column of Fig. 6) after the addition of the β_{14} term and the output spectrum yielded up to $17 \mu\text{m}$. However, the output

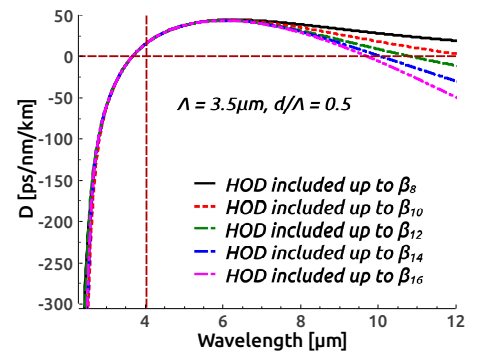


Figure 9: Comparison between data-fitted GVD curves obtained by Taylor-series expansion for the successive inclusion of HOD terms from β_8 to β_{16} . Vertical dashed line indicates pump wavelength.

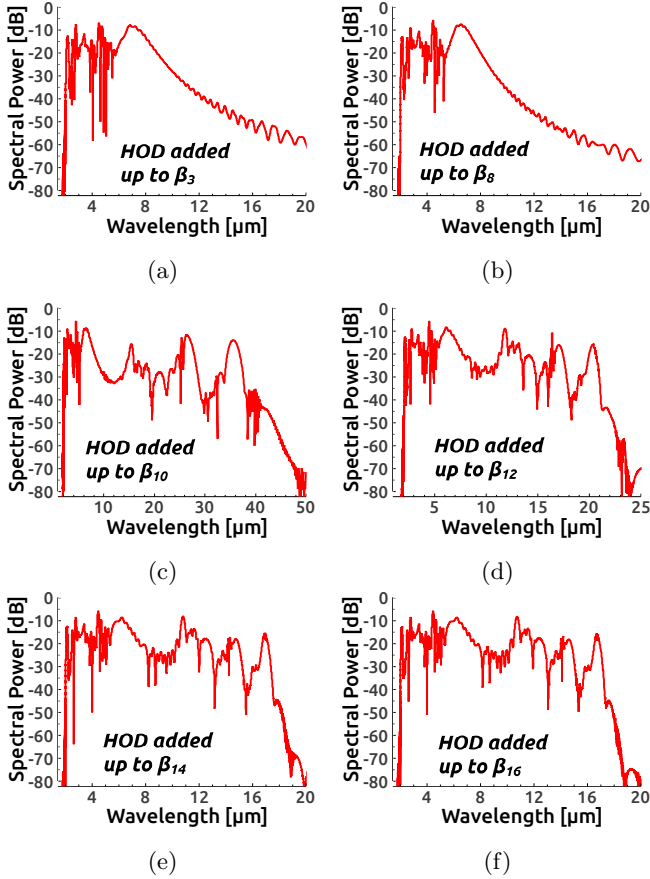


Figure 10: SC spectra at the output of As_2Se_3 PCF for the geometry of $\Lambda = 3.0 \mu\text{m}$ and $d/\Lambda = 0.5$ pumped at $3.5 \mu\text{m}$ for the HOD parameters from β_3 to β_{16} applying 3 kW peak power at the PCF input.

bandwidth does not change at the PCF output if more HOD terms (up to β_{16}) are included which is reflected in the right column of Fig. 6. The main reason behind the large SC spectra expansion at the long wavelength regime would be the nonsolitonic DW radiation which takes place as the solitons are restricted their expansion beyond the 2nd ZDW as a result of the spectral recoil effect [56]. Due to this effect, a large amount of energy transfer occurs from the soliton to the DW which eventually extends the SC spectrum beyond the $15 \mu\text{m}$. The resonant DW radiation in the anti-Stokes side remains unaltered with the further addition of more HOD terms in simulations seen in Fig. 6. The corresponding spectral and temporal evolutions exhibit qualitatively identical features except for the narrowing of the spectrum after the inclusion of certain HOD terms. Roy *et al.* [57] showed by numerical analysis the effects of including of HOD terms in the SC spectral evolution model with a phase matching condition in a PCF design. This allows for the emission of two resonant DWs separately or simultaneously by Raman solitons, depending on the sign (+ve/-ve) of the different HOD terms included. The design in this work matches that of Roy *et al.* as two DWs are emitted with the addition of cer-

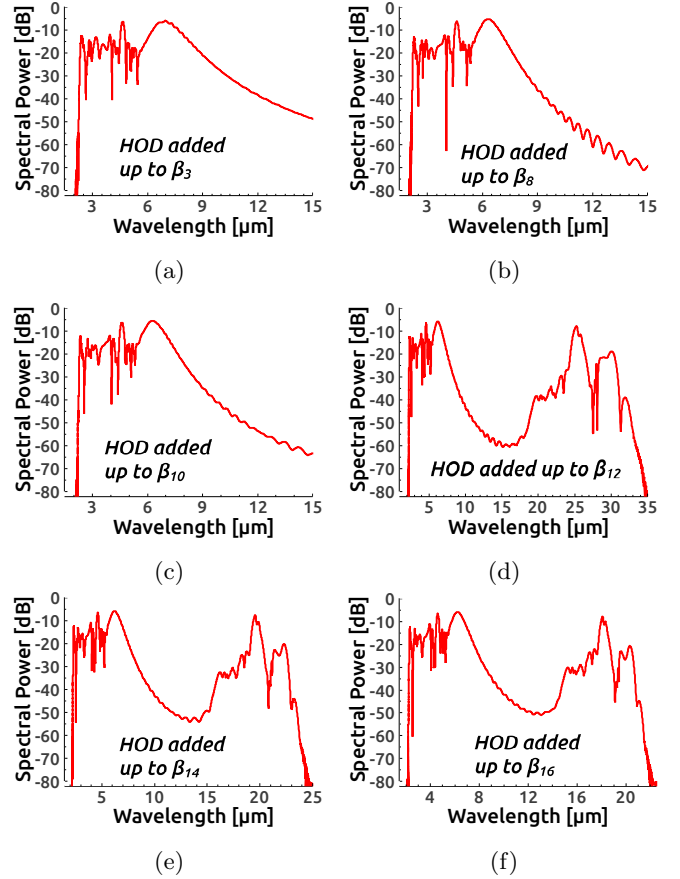


Figure 11: SC spectra at the output of As_2Se_3 PCF for the geometry of $\Lambda = 3.5 \mu\text{m}$ and $d/\Lambda = 0.5$ pumped at $4 \mu\text{m}$ for the HOD parameters from β_3 to β_{16} applying 3 kW peak power at the PCF input.

tain number of HOD terms. Moreover, the combination of all odd and even number HOD terms generates more than two DW peaks which can clearly be observed from the proposed design seen in Fig. 6. This is another reason behind the large SC spectral expansion towards the long wavelength side of the spectra. However, as observed earlier, an insufficient number of HOD terms during the SC simulations leads to spurious results at the PCF output. As such, efforts were made to ensure an adequate number of HOD terms were included into the developed simulations until spectral convergence is obtained at the PCF output. This phenomena will be explained in the next section through the Taylor-series data fitting method. As such, the proposed PCF design that contains the structural parameters, $\Lambda = 2.5 \mu\text{m}$ and $d/\Lambda = 0.6$ is the optimum design, as the SC output bandwidth does not change in this design after the inclusion of HOD terms up to β_{16} . The proposed configuration is able to produce steady SC output spanning from 2 to beyond $15 \mu\text{m}$ with the inclusion of HOD terms up to β_{14} .

The vital question is how many HOD terms that need to be calculated to yield a SC convergence at the PCF output without the successive inclusion of HOD terms during

numerical simulations. To answer this question, data fitted GVD curves are obtained through Taylor series expansion as illustrated in Fig. 7 by the successive addition of HOD terms from β_3 to β_{16} for the proposed PCF design. It is prudent to observe that in the data fitted GVD curves of Figs. 7(a)-(c), no second ZDWs on the GVD curves up to the addition of β_8 can be observed for the design. The location of 2nd ZDW can only be observed after the inclusion of β_{10} and onwards as shown in Figs. 7(d)-7(g). The 2nd ZDW of Fig. 7(d) up to the addition of β_{10} can be observed around at $10 \mu\text{m}$ wavelength. After the inclusion of more HOD terms such as β_{12} and β_{14} , the 2nd ZDW is observed to shift to the left, resulting in the anomalous dispersion region becoming narrower than earlier simulations. The addition of the term β_{16} does not change the data fitted GVD curve, as observed in Fig. 7(h). In earlier SC simulations, it was observed in Fig. 6 that the long wavelength DW moves to the left, becoming narrower as the anomalous GVD region of the data fitted GVD curve also becomes narrower up to the addition of the HOD term β_{14} . However, no spectral narrowing is observed in Fig. 6, while the 2nd ZDW of data fitted GVD curve in Fig. 7 shifts with the addition of HOD terms up to β_{16} . Thus, SC convergence can be obtained for the case with the inclusion of HOD terms up to β_{14} . In order to facilitate this discussion, a comparison between data fitted GVD curves and the GVD curve obtained by the FEM mode-solver is shown in Fig. 8 as well. It can be seen that a good agreement between the GVD curves is obtained by both methods up to the inclusion of β_{14} in data fitted curve for the proposed design. Therefore, analyzing the data fitted method shows that after evaluating the HOD parameters from the GVD curve obtained for a specific design, the data fitted method through Taylor-series expansion provides the number of HOD terms that will be required to include during SC simulations.

In order to further verify the convergence of the SC output in the proposed design, two more PCF structures are optimized for pumping at $3.5 \mu\text{m}$ and $4 \mu\text{m}$ respectively. HOD terms up to β_{16} are evaluated for both designs as well. Mode effective areas are evaluated for both geometries by the FEM mode-solver at pump wavelengths of $11.27 \mu\text{m}^2$ and $15.32 \mu\text{m}^2$ respectively resulting in corresponding nonlinear coefficients of 0.88 /W/m and 0.56 /W/m . The number of solitons, $N \approx 16$ or 6 can be calculated from L_D and L_{NL} for both designs separately. By maintaining all other parameters as before, the SC simulations are carried out for the two designs after the successive inclusion of the HOD terms up to β_{16} with the output SC results shown in Figs. 10 and 11, respectively. The same phenomena occurs for a SC evolution spanning between $2 \mu\text{m}$ and $18 \mu\text{m}$ after the inclusion of the HOD terms in the case of the PCF structure containing the dimensional parameters, $\Lambda = 3 \mu\text{m}$ and $d/\Lambda = 0.5$ which can be seen in Fig. 10. The SC bandwidth becomes stable after the addition of the β_{14} terms as shown in Fig. 10(e) and no further changes are seen to occur at the output spectrum

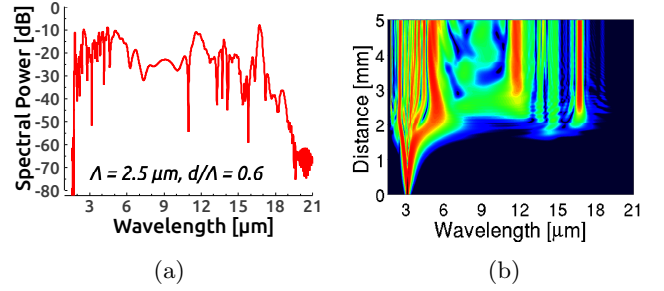


Figure 12: SC evolution at the output of 5-mm-long PCF for the geometry of $\Lambda = 2.5 \mu\text{m}$, $d/\Lambda = 0.6$ pumped at $3.1 \mu\text{m}$ with the inclusion of HOD parameters up to β_{16} applying 3 kW peak power at the PCF input.

after the inclusion of more HOD terms up to β_{16} as can be seen in Fig. 10(f). On the other hand, for the PCF geometry containing structural parameters, $\Lambda = 3.5 \mu\text{m}$ and $d/\Lambda = 0.5$, the SC spectrum extends by more than $20 \mu\text{m}$ when pumped at $4 \mu\text{m}$, inducing a small dip in the middle of the spectrum. This however may not occur in real-world applications due to long wavelength material absorption, but it can be an encouraging prediction for the proposed design. In this case, a small variation in the output bandwidth is observed between β_{14} and β_{16} as seen in Figs. 11(e) and 11(f). As the 2nd ZDW of this PCF structure is located at around $10 \mu\text{m}$, which is shifted to the right resulting in wider anomalous dispersion region than that observed for the case of the 2nd ZDWs of earlier two designs, thus, a wider SC bandwidth/extension is realized in this case as compared to earlier designs. This is also verified with data fitted GVD curve shown in Fig. 9 after the inclusion of β_{16} and a small difference is observed between the data fitted GVD curve and the GVD curve obtained by the FEM mode-solver. Thus, in order to achieve a stable and steady SC output in the case of PCF geometry containing the dimensional parameters, $\Lambda = 3.5 \mu\text{m}$ and $d/\Lambda = 0.5$, the HOD parameters up to β_{16} must be included during numerical simulations.

Since the propagation loss increases with the waveguide length and to keep the loss reasonably low, a 20-mm-long PCF is considered during entire SC simulations in this

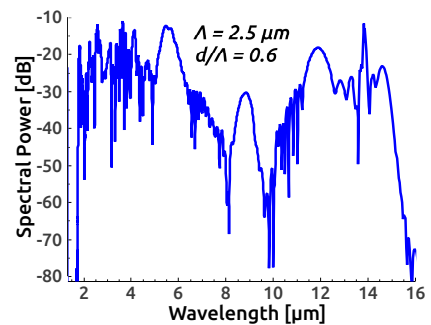


Figure 13: Output SC for a PCF structure of $\Lambda = 2.5 \mu\text{m}$, $d/\Lambda = 0.6$ by considering linear propagation loss of 2 dB/cm with a low peak power of 3 kW.

work. Numerical analyses show that almost an identical SC bandwidth, illustrated in Fig. 12, can be achieved for a 20-mm-long PCF if the PCF length is reduced to 5-mm or even less. For such a short waveguide design, the loss will be reduced significantly than earlier designs and may be even become negligible resulting in an unaltered SC spectral evolutions at the waveguide output. However, the SC bandwidth would eventually decrease somewhat owing to long wavelength material absorption from the simulated values at the PCF output as wavelength independent propagation loss is considered during all numerical simulations. Moreover, the impact of a high linear absorption edge after 17 μm of As_2Se_3 material may also clamp further SC spectral broadening at the PCF output. Wang *et al.* [34] recently reported MIR region SC generation using a 12-cm-long As_2Se_3 step-index fiber with a measured average transmission loss of 4 dB/m between 2.5 μm and 12 μm with three strong absorption peaks of O-H, As-O and Se-O located around at 2.7 μm , 8.2 μm and 10.5 μm , respectively. To see the impact of long wavelength absorption loss on SC bandwidth at the PCF output, numerical simulations are performed for the proposed structures by arbitrarily increasing the linear propagation loss from 0.65 dB/cm to 2 dB/cm, giving simulated result in Fig. 13. It can be seen from figure that the SC spectral evolution at the PCF output still can be obtained up to 15 μm (bandwidth evaluated at -40 dB from the peak) by adopting a more conservative approach towards increasing linear absorption loss more than three times with the same low peak power of 3 kW.

To date, the widest SC broadening was reported through numerical simulation by Saini *et al.*, spanning the wavelength range from 2 to 15 μm in a 5-mm long triangular core graded index As_2Se_3 PCF pumped at 4.1 μm with a peak power of 3.5 kW [33], while Karim *et al.* recently numerically reported ultrabroadband MIR SC generation covering the wavelength range 2.3–15 μm using a 10-mm-long all-ChG triangular core microstructured fiber (Ge-AsSe/GeAsS) when pumped at 4 μm with a pulse duration of 100-fs and a low peak power of 3 kW [37]. The broadest experimental demonstration of a MIR SC spectrum was reported using a 3-cm-long $\text{As}_2\text{Se}_3/\text{AsSe}_2$ step-index fiber by Cheng *et al.*, covering the range from 2 to 15.1 μm , when pumped by a 9.8 μm signal with a peak power of 2.89 MW [13]. On the other hand, Zhao *et al.* experimentally demonstrated MIR SC generation spanning from 2 to 16 μm using a 14-cm-long tellurite based step-index fiber. This however required the use of a pulsed seed signal at 7 μm with a 150-fs pulse width, repetition rate of 1 kHz and a peak power of 77 MW in the normal dispersion regime [4]. In the proposed design, which is based on a typical hexagonal As_2Se_3 PCF structure, it would be theoretically possible to obtain the broadest SC expansion yet in the MIR region, extending beyond 17 μm using a pump signal at 3.1 μm with a much lower peak power of 3 kW. However, the SC bandwidth may actually be lower when demonstrated experimentally due to additional coupling

losses between the pump source and the PCF structure. Alternatively, the peak power can be increased slightly to compensate for the coupling losses.

4. Concluding remarks

In this numerical work, an As_2Se_3 based chalcogenide PCF for ultrabroadband SC generation in the MIR region is numerically proposed and analyzed. A 20-mm-long hexagonal PCF geometry is proposed and optimized by varying its d and Λ structural parameters. Four designs with different dimensional parameters are optimized for pumping at 2.05 μm , 3.1 μm , 3.5 μm and 4 μm , respectively. Using the first proposed design, which is optimized for pumping at 2.05 μm , a SC spectral evolution up to 6 μm with a peak power of 100 W is obtained. It is possible to achieve such a broadband MIR spanning with a much low peak power only due to the small core size which helps to produce large nonlinear coefficient inside the PCF. In this case, the convergence of SC output is obtained with the addition of HOD terms up to β_{10} . To further increase the SC spectrum into the MIR, the pump wavelength is shifted between 3.1 and 4 μm and optimized three more designs for pumping them at these wavelengths by raising the pulse peak power at 3 kW. Using this peak power, an ultrabroadband SC can be realized spanning from 2 to beyond 15 μm by the proposed 2nd PCF geometry containing the dimensional parameters, $\Lambda = 2.5 \mu\text{m}$ and $d/\Lambda = 0.6$. In this design, initially, HOD terms up to β_{10} are included during SC simulation which results in spurious SC bandwidth at the PCF output. To obtain a spurious free SC output by the optimized design, HOD terms up to β_{16} are evaluated and successively included into numerical simulations. The SC output converges with the addition of HOD terms up to β_{14} for the PCF structure containing structural parameters of Λ between 2.5 μm and 3 μm and d/Λ between 0.5 and 0.6. However, in the case of the PCF geometry containing, $\Lambda = 3.5 \mu\text{m}$ and $d/\Lambda = 0.5$, the HOD terms of up to β_{16} are required for predicting a stable SC output during numerical simulations. This phenomena can also be verified for a specific design by data fitted GVD curves where the actual GVD curve converges closely with the data fitted GVD curve which can be evaluated after the inclusion of certain HOD terms determined through Taylor series expansion. Therefore, for any design optimized with certain structural parameters and pump wavelength, the number of HOD terms required for a convergence of SC at the waveguide output can be predicted by matching the actual GVD curve obtained through the FEM mode-solver with the data fitted GVD curve after including the certain HOD terms into the data fitted method through Taylor-series expansion.

Until today, many researchers demonstrated SC generation numerically by including different number of HOD terms into their simulation works. From those works it is hard to predict the number of necessary HOD terms that required to obtain steady SC output for a specific

design. In this paper, a proposed PCF model is designed through dispersion engineering for predicting a spurious free MIR SC generation by systematic analysis of HOD parameters that required to include during numerical simulations where the number of HOD terms are determined through the convergence of Taylor series approximation with increasing fitting parameters. The proposed model is designed based on a conventional As_2Se_3 hexagonal PCF, which can be used to generate an ultrabroadband MIR SC spectral broadening spanning from $2\ \mu\text{m}$ to beyond $15\ \mu\text{m}$ with a low peak power of 3 kW, and has significant potential to be employed in several MIR region applications.

5. ACKNOWLEDGEMENT

Funding for this research was provided by the Ministry of Higher Education (MOHE) under the grants GA 010-2014 (ULUNG) and the University of Malaya under the grants RP029B-15 AFR and RU001-2017.

References

- [1] J. M. Dudley, G. Genty, and S. Coen, Supercontinuum generation in photonic crystal fiber, *Rev. Mod. Phys.* 78 (2006) 1135–1184.
- [2] A. B. Seddon, A prospective for new mid-infrared medical endoscopy using chalcogenide glasses, *Int. J. Appl. Glass Sci.* 3 (2011) 177–191.
- [3] A. Schliesser, N. Picque, and T. W. Haensch, Mid-infrared frequency combs, *Nat. Photonics* 6 (2012) 440–449.
- [4] Z. Zhao, B. Wu, X. Wang, Z. Pan, Z. Liu, P. Zhang, X. Shen, Q. Nie, S. Dai, and R. Wang, Mid-infrared supercontinuum covering 2–16 μm in a low-loss telluride single-mode fiber, *Laser Photonics Rev.* 2 (2017) 1700005.
- [5] J. Swiderski and M. Michalska, High-power supercontinuum generation in a ZBLAN fiber with very efficient power distribution toward the mid-infrared, *Opt. Lett.* 39 (2014) 910–913.
- [6] M. Liao, G. Qin, X. Yan, T. Suzuki, and Y. Ohishi, A Tellurite nanowire with long suspended struts for low-threshold single-mode supercontinuum generation, *J. Lightwave Technol.* 29 (2011) 194–199.
- [7] T. Cheng, L. Zhang, X. Xue, D. Deng, T. Suzuki, and Y. Ohishi, Broadband cascaded four-wave mixing and supercontinuum generation in a tellurite microstructured optical fiber pumped at 2 μm , *Opt. Express* 23 (2015) 4125–4134.
- [8] W. Gao, M. E. Amraoui, M. Liao, H. Kawashima, Z. Duan, D. Deng, T. Cheng, T. Suzuki, Y. Messaddeq, and Y. Ohishi, Mid-infrared supercontinuum generation in a suspended-core As_2S_3 chalcogenide microstructured optical fiber, *Opt. Express* 21 (2013) 9573–9583.
- [9] J. J. Pigeon, S. Ya. Tochitsky, C. Gong, and C. Joshi, Supercontinuum generation from 2 to 20 μm in GaAs pumped by picosecond CO_2 laser pulses, *Opt. Lett.* 39 (2014) 3246–3249.
- [10] Y. Yu, X. Gai, P. Ma, K. Vu, Z. Yang, R. Wang, D. Choi, S. Madden, and B. Luther-Davies, Experimental demonstration of linearly polarized 2–10 μm supercontinuum generation in a chalcogenide rib waveguide, *Opt. Lett.* 41 (2016) 958–961.
- [11] C. R. Petersen, U. Møller, I. Kubat, B. Zhou, S. Dupont, J. Ramsay, T. Benson, S. Sujecki, M. Abdel-Moneim, Z. Tang, D. Furniss, A. Seddon, and O. Bang, Mid-infrared supercontinuum covering the 1.4–13.3 μm molecular fingerprint region using ultra-high NA chalcogenide step-index fiber, *Nat. Photonics* 8 (2014) 830–834.
- [12] Y. Yu, B. Zhang, X. Gai, C. Zhai, S. Qi, W. Guo, Z. Yang, R. Wang, D. Choi, S. Madden, and B. Luther-Davies, 1.8–10 μm mid-infrared supercontinuum generated in a step-index chalcogenide fiber using low peak pump power, *Opt. Lett.* 40 (2015) 1081–1084.
- [13] T. Cheng, K. Nagasaka, T. H. Tuan, X. Xue, M. Matsumoto, H. Tezuka, T. Suzuki, and Y. Ohishi, Mid-infrared supercontinuum generation spanning 2 to 15.1 μm in a chalcogenide step-index fiber, *Opt. Lett.* 41 (2016) 2117–2120.
- [14] H. Ou, S. Dai, P. Zhang, Z. Liu, X. Wang, F. Chen, H. Xu, B. Luo, Y. Huang, and R. Wang, Ultrabroad supercontinuum generated from a highly nonlinear GeSbSe fiber, *Opt. Lett.* 41 (2016) 3201–3204.
- [15] G. Qin, X. Yan, C. Kito, M. Liao, C. Chaudhari, T. Suzuki, and Y. Ohishi, Ultrabroadband supercontinuum generation from ultraviolet to 6.28 μm in a fluoride fiber, *Appl. Phys. Lett.* 95 (2009) 161103.
- [16] P. Domachuk, N. A. Wolchover, M. Cronin-Golomb, A. Wang, A. K. George, C. M. B. Cordeiro, J. C. Knight, and F. G. Omenetto, Over 4000 nm bandwidth of Mid-IR supercontinuum generation in subcentimeter segments of highly nonlinear tellurite PCFs, *Opt. Express* 16 (2008) 7161–7168.
- [17] X. Gai, T. Han, A. Prasad, S. Madden, D. Y. Choi, R. Wang, D. Bulla, and B. Luther-Davies, Progress in optical waveguides fabricated from chalcogenide glasses, *Opt. Express* 18 (2010) 26635–26646.
- [18] D. D. Hudson, E. C. Mägi, A. C. Judge, S. A. Dekker, and B. J. Eggleton, Highly nonlinear chalcogenide glass micro/nanofiber devices: Design, theory, and octave-spanning spectral generation, *Opt. Commun.* 285 (2012) 4660–4669.
- [19] L. Petit, N. Carlie, K. Richardson, A. Humeau, S. Cherukulapurath, and G. Boudebs, Nonlinear optical properties of glasses in the system Ge/Ga-Sb-S/Se, *Opt. Lett.* 31 (2006) 1495–1497, 2006.
- [20] E. C. Magi, L. B. Fu, H. C. Nguyen, M. R. E. Lamont, D. I. Yeom, and B. J. Eggleton, Enhanced Kerr nonlinearity in sub-wavelength diameter As_2Se_3 chalcogenide fiber tapers, *Opt. Express* 15 (2007) 10324–10329.
- [21] A. Al-Kadry, M. E. Amraoui, Y. Messaddeq, and M. Rochette, Two octaves mid-infrared supercontinuum generation in As_2Se_3 microwires, *Opt. Express* 22 (2014) 31131–31137.
- [22] I. Kubat, C. S. Agger, U. Moller, A. B. Seddon, Z. Tang, S. Sujecki, T. M. Benson, D. Furniss, S. Lamarini, K. Scholle, P. Fuhrberg, B. Napier, M. Farries, J. Ward, P. M. Moselund, and O. Bang, Mid-infrared supercontinuum generation to 12.5 μm in large NA chalcogenide step-index fibers pumped at 4.5 μm , *Opt. Express* 22 (2014) 19169–19182.
- [23] C. Wei, X. Zhu, R. A. Norwood, F. Seng, and N. Peyghambarian, Numerical investigation on high power mid-infrared supercontinuum fiber lasers pumped at 3 μm , *Opt. Express* 24 (2013) 29488–29504.
- [24] B. J. Eggleton, B. Luther-Davies, and K. Richardson, Chalcogenide photonics, *Nat. Photonics* 5 (2011) 141–148.
- [25] I. D. Aggarwal and J. S. Sanghera, Development and applications of chalcogenide glass optical fibers at NRL, *J. Optoelectron. Adv. Mater.* 4 (2002) 665–678.
- [26] J. Sanghera, C. Florea, L. Shaw, P. Pureza, V. Nguyen, M. Bashkansky, Z. Dutton, and I. Aggarwal, Non-linear properties of chalcogenide glasses and fibers, *J. Non-Cryst. Solids* 354 (2008) 462.
- [27] P. Ma, D. Y. Choi, Y. Yu, X. Gai, Z. Yang, S. Debbarma, S. Madden, and B. Luther-Davies, Low-loss chalcogenide waveguides for chemical sensing in the mid-infrared, *Opt. Express* 21 (2013) 29927–29937.
- [28] L. B. Shaw, R. R. Gattass, J. S. Sanghera, and I. D. Aggarwal, All-fiber mid-IR supercontinuum source from 1.5 to 5 μm , *Proc. SPIE* 7914 (2011) 1–5.
- [29] J. Hu, C. R. Menyuk, L. B. Shaw, J. S. Sanghera, and I. D. Aggarwal, Maximizing the bandwidth of supercontinuum generation in As_2Se_3 chalcogenide fibers, *Opt. Express* 18 (2010) 6722–6739.
- [30] U. Møller, Y. Yu, I. Kubat, C. R. Petersen, X. Gai, L. Brilland, D. Mechin, C. Caillaud, J. Troles, B. Luther-Davies, and O.

- Bang, Multi-milliwatt mid-infrared supercontinuum generation in a suspended core chalcogenide fiber, *Opt. Express* 23 (2015) 3282–3291.
- [31] C. R. Petersen, R. D. Engelsholm, C. Markos, L. Brilland, C. Caillaud, J. Troles, and O. Bang, Increased mid-infrared supercontinuum bandwidth and average power by tapering large-mode-area chalcogenide photonic crystal fibers, *Opt. Express* 25 (2017) 15336–15348.
- [32] D. D. Hudson, S. Antipov, L. Li, I. Alamgir, T. Hu, M. El-Amraoui, Y. Messaddeq, M. Rochette, S. D. Jackson, and A. Fuerbach, Toward all-fiber supercontinuum spanning the mid-infrared, *Optica* 4 (2017) 1163–1166.
- [33] T. S. Saini, A. Kumar, and R. K. Sinha, Broadband mid-infrared supercontinuum spectra spanning 2–15 μm using As_2Se_3 chalcogenide glass triangular-core graded-index photonic crystal fiber, *J. Lightw. Technol.* 33 (2015) 3914–3920.
- [34] Y. Wang, S. Dai, X. Han, P. Zhang, Y. Liu, X. Wang, and S. Sun, Broadband mid-infrared supercontinuum generation in novel As_2Se_3 - $\text{As}_2\text{Se}_2\text{S}$ step-index fibers, *Opt. Comm.* 410 (2018) 410–415.
- [35] C. Markos, J. C. Travers, A. Abdolvand, B. J. Eggleton, and O. Bang, Hybrid photonic-crystal fiber, *Rev. Mod. Phys.* 89(4) (2017) 045003.
- [36] M. S. Habib, C. Markos, O. Bang, and M. Bache, Soliton-plasma nonlinear dynamics in mid-IR gas-filled hollow-core fibers, *Opt. Lett.* 42 (2017) 2232–2235.
- [37] M. R. Karim, H. Ahmad, and B. M. A. Rahman, Design and modeling of dispersion-engineered all-chalcogenide triangular-core fiber for mid-infrared-region supercontinuum generation, *J. Opt. Soc. Am. B* 35 (2018) 266–275.
- [38] J. Fatome, C. Fortier, T. N. Nguyen, T. Chartier, F. Smektala, K. Messaad, B. Kibler, S. Pitois, G. Gadret, C. Finot, J. Troles, F. Desevedavy, P. Houizot, G. Renversez, L. Brilland, and N. Traynor, “Linear and nonlinear characterizations of chalcogenide photonic crystal fibers, *J. Lightwave Technol.* 27 (2009) 1707–1715.
- [39] J. C. Knight, T. A. Birks, P. S. Russell, and D. M. Atkin, All-silica single-mode optical fiber with photonic crystal cladding, *Opt. Lett.* 21 (1996) 1547–1549.
- [40] R. F. Cregan, B. J. Mangan, J. C. Knight, T. A. Birks, P. S. Russell, P. J. Roberts, and D. C. Allan, Single-mode photonic band gap guidance of light in air, *Science* 5433 (1999) 1537–1539.
- [41] J. C. Knight and P. S. J. Russell, Photonic crystal fibers: New way to guide light, *Science* 296 (2002) 276–277.
- [42] K. Tajima, J. Zhou, K. Nakajima, and K. Sato, Ultra low loss and long length photonic crystal fiber, *J. Lightwave Technol.* 22 (2004) 7–10.
- [43] L. Brilland, F. Smektala, G. Renversez, T. Chartier, J. Troles, T. N. Nguyen, N. Traynor, and A. Monteville, Fabrication of complex structures of Holey Fibers in chalcogenide glasses, *Opt. Express* 14 (2006) 1280–1285.
- [44] V. Shiryayev and M. Churbanov, Trends and prospects for development of chalcogenide fibers for mid-infrared transmission, *J. Non-Cryst. Solids* 377 (2013) 225–230.
- [45] M. R. Karim, B. M. A. Rahman, and G. P. Agrawal, Dispersion engineered $\text{Ge}_{11.5}\text{As}_{24}\text{Se}_{64.5}$ nanowire for supercontinuum generation: A parametric study, *Opt. Express* 22 (2014) 31029–31040.
- [46] K. M. Mohsin, M. S. Alam, D. M. N. Hasan, and M. N. Hossain, Dispersion and nonlinearity properties of a chalcogenide As_2Se_3 suspended core fiber, *Appl. Opt.* 50 (2011) E102–E107.
- [47] B. M. A. Rahman and J. B. Davies, Finite-element solution of integrated optical waveguides, *J. Lightwave Technol.* 2 (1984) 682–688.
- [48] G. P. Agrawal, *Nonlinear Fiber Optics*, 5th ed. (Academic, Elsevier, 2013).
- [49] M. R. Karim, B. M. A. Rahman, Y. O. Azabi, A. Agrawal, and G. P. Agrawal, Ultra-broadband mid-infrared supercontinuum generation through dispersion engineering of chalcogenide microstructured fibers, *J. Opt. Soc. Am. B* 32 (2015) 2343–2351.
- [50] L. Liu, T. Cheng, K. Nagasaka, H. Tong, G. Qin, T. Suzuki, and Y. Ohishi, Coherent mid-infrared supercontinuum generation in all-solid chalcogenide microstructured fibers with all-normal dispersion, *Opt. Lett.* 41 (2016) 392–395.
- [51] M. R. Karim, H. Ahmad, and B. M. A. Rahman, All-normal dispersion chalcogenide PCF for ultraflat mid-infrared supercontinuum generation, *IEEE Photonics Technol. Lett.* 29(21) (2017) 1792–1795.
- [52] S. Xing, D. Grassani, S. Kharitonov, A. Billat, and C-S. Bres, Characterization and modeling of microstructured chalcogenide fibers for efficient mid-infrared wavelength conversion, *Opt. Express* 24 (2016) 9741–9750.
- [53] S. Xing, D. Grassani, S. Kharitonov, L. Brilland, C. Caillaud, J. Troles, and C-S. Bres, Mid-infrared continuous-wave parametric amplification in chalcogenide microstructured fibers, *Optica* 4 (2017) 643–648.
- [54] P. Toupin, L. Brilland, J. Troles, and J. -L. Adam, Small core Ge-As-Se microstructured optical fiber with single-mode propagation and low optical losses, *Opt. Mater. Express* 2 (2012) 1359–1366.
- [55] Y. Tang, L. G. Wright, K. Charan, T. Wang, C. Xu, and F. W. Wise, Generation of intense 100-fs solitons tunable from 2 to 4.3 μm in fluoride fiber, *Optica* 3 (2016) 948–951.
- [56] F. Biancalana, D. V. Skryabin, and A. V. Yulin, Theory of the soliton self-frequency shift compensation by resonant radiation in photonic crystal fibers, *Physical Review E* 70 (2004) 016615.
- [57] S. Roy, S. K. Bhadra, and G. P. Agrawal, Effects of higher-order dispersion on resonant dispersive waves emitted by solitons, *Opt. Lett.* 34 (2009) 2072–2074.